Rarefied Gas Flow over a Double Airfoil Configuration

Prepared by: Ohad Haftka
Student ID: 212489728
Advisor: Prof. Avshalom Manela

April 24, 2025

Contents

1 Introduction

Understanding the dynamics of rarefied gas flow is essential to predict aerodynamic forces in low-density environments, such as the upper atmosphere [1]. This is particularly relevant for low Earth orbit satellites, where forces due to rarefied gas interactions can significantly influence satellite trajectories and orientation [2]. The insights gained from this study can be applied to enhance the accuracy of force predictions and improve the design and operation of satellite systems.

Rarefied gas flow also plays a crucial role in various engineering applications, such as micro-fluidics and vacuum technologies, where conventional continuum assumptions break down [3]. By modeling these interactions accurately, it becomes possible to predict flow behavior in highly rarefied regimes, providing a bridge between molecular dynamics and macroscopic fluid behavior [4].

2 Problem Description

This project investigates a steady-state rarefied gas flow over two straight, parallel airfoils of length L^*, separated by a distance D^*. The top airfoil is maintained at a temperature T_t^*, while the bottom airfoil has a temperature T_b^*. A uniform flow enters the system with density ρ_∞^*, temperature T_∞^*, and velocity $\mathbf{u}_\infty^* = (u_{\infty,x}^*, u_{\infty,y}^*, 0)$. Each gas particle has a mass m^*. The flow interactions between the airfoil and the boundaries are modeled using diffuse boundary conditions to predict aerodynamic behavior.

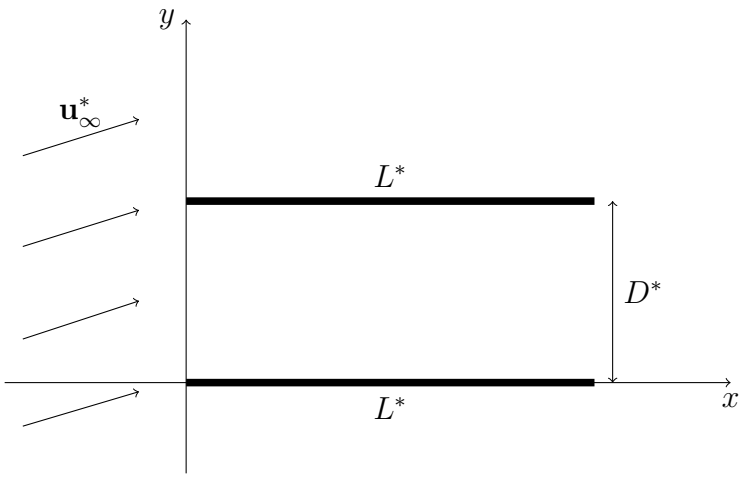

Figure 1: Schematic of the problem configuration.

3 Mathematical Problem

3.1 The Boltzmann Equation

The behavior of the rarefied gas is governed by the full Boltzmann equation:

$$\frac{\partial f^*}{\partial t^*} + \boldsymbol{\xi}^* \cdot \nabla f^* + \frac{\mathbf{X_0}^*}{m^*} \cdot \frac{\partial f^*}{\partial \boldsymbol{\xi}^*} = J \tag{1}$$

where f^* is the distribution function, $\boldsymbol{\xi}^*$ is the molecular velocity, $\mathbf{X_0}^*$ is the external force, and J is the collision operator. For steady-state conditions and negligible external forces, equation 1 reduces to:

$$\boldsymbol{\xi}^* \cdot \nabla f^* = J \tag{2}$$

After normalization, and assuming the ballistic limit ($J \to 0$), equation 2 simplifies to:

$$\boldsymbol{\xi} \cdot \nabla f = 0 \tag{3}$$

Here, dimensionless variables such as $\boldsymbol{\xi} = \boldsymbol{\xi}^*/\sqrt{2R^*T_\infty^*}$ and $f = f^*/(\rho_\infty^*/(2\pi R^*T_\infty^*)^{3/2})$ have been introduced while the other normalizations will take place using these relations:

- $d = D^*/L^*$
- $\tau_t = T_t^*/T_\infty^*$
- $\tau_b = T_b^*/T_\infty^*$
- $\rho_j = \rho_j^*/\rho_\infty^*$
- $\boldsymbol{u}_\infty = \boldsymbol{u_\infty}^*/\sqrt{2R^*T_\infty^*}$

3.2 Boundary Conditions and Diffuse Wall Assumption

The diffuse wall boundary condition assumes particles are re-emitted from surfaces with a Maxwellian distribution corresponding to the wall's temperature and velocity which, in our case, is zero:

$$f_w^* = \frac{\rho_w^*}{(2\pi R^*T_w^*)^{3/2}} \exp\left(-\frac{(\boldsymbol{\xi}^* - \boldsymbol{u_w}^*)^2}{2R^*T_w^*}\right). \tag{4}$$

This implies that there is no memory of the direction of the incoming particles, with properties solely dependent on the wall. Similarly, particles originating from the free flow, rather than being re-emitted by the walls, also follow a Maxwellian distribution with $T^* = T_\infty^*$ and $\mathbf{u}^* = \mathbf{u}_\infty{}^*$. Note that ρ_w^* is not an actual density property of the wall, but rather a parameter calculated for each point on the wall to ensure compliance with impermeability conditions. Since each side of each airfoil is subject to different conditions, I conclude that each airfoil has two re-emission distributions differing by the property ρ_w^*. Thus, the following notation will be used from now on: the subscript t will refer to the top airfoil as with the temperatures, whereas b will be used for the bottom airfoil. The subscript o denotes the outer side of each airfoil, and i refers to the inner side. After accounting for the normalizations, I can use the notation for the boundary conditions using equation 4:

- $f_\infty = \pi^{-\frac{3}{2}} e^{-(\boldsymbol{\xi} - \boldsymbol{u_w})^2}$
- $f_{to} = \rho_{to}\tau_t^{-\frac{3}{2}}\pi^{-\frac{3}{2}} e^{-\boldsymbol{\xi}^2/\tau_t}$
- $f_{ti} = \rho_{ti}\tau_t^{-\frac{3}{2}}\pi^{-\frac{3}{2}} e^{-\boldsymbol{\xi}^2/\tau_t}$
- $f_{bo} = \rho_{bo}\tau_b^{-\frac{3}{2}}\pi^{-\frac{3}{2}} e^{-\boldsymbol{\xi}^2/\tau_b}$
- $f_{bi} = \rho_{bi}\tau_b^{-\frac{3}{2}}\pi^{-\frac{3}{2}} e^{-\boldsymbol{\xi}^2/\tau_b}$

3.3 Solution Form

The solution to this form of the Boltzmann equation 3 is that for every point in the space the probability distribution of finding a particle with a certain velocity $\boldsymbol{\xi}$ is equal to the distribution of the boundary condition from which the velocity $\boldsymbol{\xi}$ originates. For example, let us focus on the area in between the two airfoils (case 4).

$$f(x_1, y_1, \boldsymbol{\xi}) = \begin{cases} f_\infty & \text{if } \xi_x > 0 \quad \text{and} \quad \frac{y_1-d}{x_1}\xi_x < \xi_y < \frac{y_1}{x_1}\xi_x \\ & \text{or} \\ & \text{if } \xi_x < 0 \quad \text{and} \quad \frac{y_1-d}{x_1-1}\xi_x < \xi_y < \frac{y_1}{x_1-1}\xi_x \\ f_{ti} & \text{if } \xi_y < 0 \quad \text{and} \quad \frac{x_1}{y_1-d}\xi_y < \xi_x < \frac{x_1-1}{y_1-d}\xi_y \\ f_{bi} & \text{if } \xi_y > 0 \quad \text{and} \quad \frac{x_1-1}{y_1}\xi_y < \xi_x < \frac{x_1}{y_1}\xi_y \end{cases} \tag{5}$$

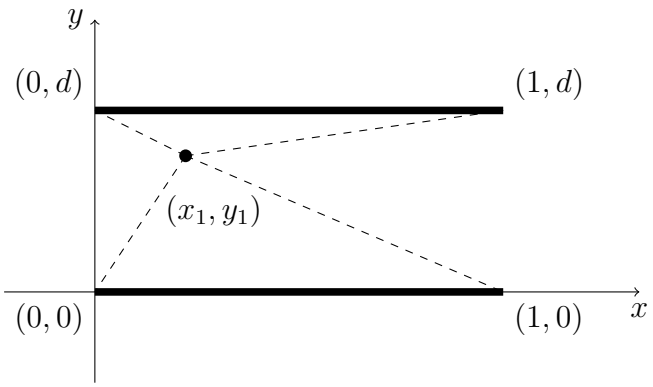

Figure 2: possible origins of particles based on molecular velocity for a point between the two airfoils

While an example for a point above the top airfoil might look like this (case 2):

$$f(x_1, y_1, \boldsymbol{\xi}) = \begin{cases} f_{to} & \text{if } \xi_y > 0 \quad \text{and} \quad \frac{x_1-1}{y_1-d}\xi_y < \xi_x < \frac{x_1}{y_1-d}\xi_y \\ f_{bi} & \text{if } \xi_y > 0 \quad \text{and} \quad \frac{x_1-1}{y_1}\xi_y < \xi_x < \frac{x_1-1}{y_1-d}\xi_y \\ f_\infty & \text{otherwise} \end{cases} \tag{6}$$

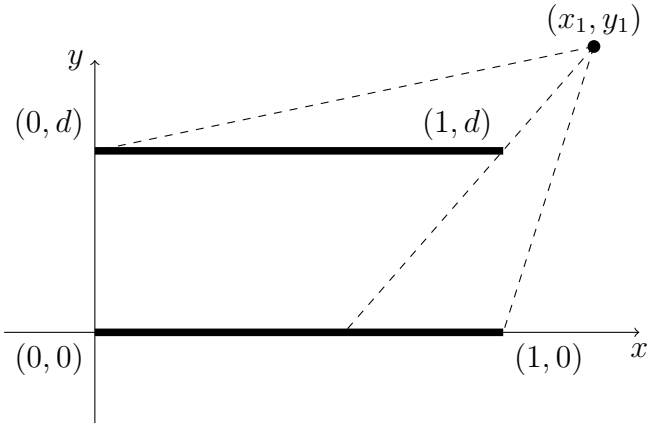

Figure 3: possible origins of particles based on molecular velocity for a point above the top airfoil

Therefore the only thing now needed to obtain the entire field f at any point in space are the unknowns $\rho_{to}, \rho_{ti}, \rho_{bi}$ and ρ_{bo}. Also caution need to take place when defining the setting the sections boundaries to avoid overlaps. in appendix A there is an explanation of the different cases for different points in space.

4 Analytical Process

4.1 impermeability conditions

In order to enforce the impermeability conditions, I will evaluate the macroscopic velocity of the gas at $y = 0$ and at $y = d$ while using the four unknown functions $\rho_{to}(x), \rho_{ti}(x), \rho_{bi}(x), \rho_{bo}(x)$ and set the expression to be equal zero. Using the solution form from section 3.3 and plugging in $y_1 = 0$ or $y_1 = d$ the distribution f can be found. now it can be used together with the formula for the macroscopic velocity from section 4.2 to get the velosity. applying those steps for the top outer surface (case 1 with $y_1 = d$) I get the following equation:

$$\int_{-\infty}^{\infty}\int_{0}^{\infty}\int_{-\infty}^{\infty} \xi_y f_{to}\, d\xi_x\, d\xi_y\, d\xi_z + \int_{-\infty}^{\infty}\int_{-\infty}^{0}\int_{-\infty}^{\infty} \xi_y f_{\infty}\, d\xi_x\, d\xi_y\, d\xi_z = 0 \tag{7}$$

Using the relations in section 3.2 I get

$$\int_{-\infty}^{\infty}\int_{0}^{\infty}\int_{-\infty}^{\infty} \xi_y \rho_{to} \tau_t^{-3/2} \pi^{-3/2} e^{-\boldsymbol{\xi}^2/\tau_t}\, d\xi_x\, d\xi_y\, d\xi_z + \int_{-\infty}^{\infty}\int_{-\infty}^{0}\int_{-\infty}^{\infty} \xi_y \pi^{-3/2} e^{-(\boldsymbol{u}--\boldsymbol{\xi})^2}\, d\xi_x\, d\xi_y\, d\xi_z = 0 \tag{8}$$

and after simplification:

$$\rho_{to} = 2\tau_t^{-1/2}(\beta_{-\infty} - \beta_0) \tag{9}$$

where

$$\beta_a = -\frac{1}{2} u_{y\infty}\sqrt{\pi}\,\mathrm{erf}(u_{y\infty} - a) - \frac{1}{2} e^{-(a-u_y)^2} \tag{10}$$

and in a similar fashion for the bottom outer surface:

$$\rho_{bo} = 2\tau_b^{-1/2}(\beta_{\infty} - \beta_0) \tag{11}$$

Note that these expressions are constant and do not change throughout the length of the airfoil. Now for the inner surfaces, starting withe the top one through the same process of using the solution form (case 4 and $y_1 = 1$), plug in from section 3.2 and simplifying I receive:

$$\begin{aligned} &\frac{1}{2\sqrt{\pi}}\left\{2(\beta_{\infty} - \beta_0) + \int_0^{\infty} \gamma(\frac{x_1}{d}) d\xi_y - \int_0^{\infty} \gamma(\frac{x_1 - 1}{d}) d\xi_y\right\} + \\ &\frac{1}{\tau_b \pi}\int_0^{\infty} \xi_y e^{-\xi_y^2/\tau_b} \left\{\int_{\frac{x_1-1}{d}\xi_y}^{\frac{x_1}{d}\xi_y} \rho_{bi}(x_1 - \frac{\xi_x}{\xi_y} d) e^{-\xi_x^2/\tau_b} d\xi_x\right\} d\xi_y + \\ &-\frac{1}{2}\rho_{ti}(x_1)\sqrt{\frac{\tau_t}{\pi}} = 0 \end{aligned} \tag{12}$$

where

$$\gamma(a) = \xi_y\,\mathrm{erf}(u_{x\infty} - a\xi_y) e^{-(u_{y\infty} - \xi_y)^2} \tag{13}$$

Now I can switch the integrating parameter to be $x_2 = x_1 - \frac{\xi_x}{\xi_y} d$ and not forgetting the Jacobian I can get together with the equation for the inner bottom surface this system of equations:

$$\begin{cases} \rho_{ti}(x_1) = g_1(\rho_{bi}, x_1) = \dfrac{2}{\sqrt{\tau_t}} \left\{ \dfrac{1}{4d}\sqrt{\tau_b} \displaystyle\int_0^1 \rho_{bi}(x_2) \left[\left(\frac{x_1 - x_2}{d} \right)^2 + 1 \right]^{-3/2} dx_2 \right. \\ \qquad \left. + \dfrac{1}{2} \left[2(\beta_\infty - \beta_0) + \displaystyle\int_0^\infty \gamma\left(\frac{x_1}{d}\right) d\xi_y - \int_0^\infty \gamma\left(\frac{x_1 - 1}{d}\right) d\xi_y \right] \right\} \\ \rho_{bi}(x_1) = g_2(\rho_{ti}, x_1) = \dfrac{2}{\sqrt{\tau_b}} \left\{ \dfrac{1}{4d}\sqrt{\tau_t} \displaystyle\int_0^1 \rho_{ti}(x_2) \left[\left(\frac{x_1 - x_2}{d} \right)^2 + 1 \right]^{-3/2} dx_2 \right. \\ \qquad \left. - \dfrac{1}{2} \left[2(\beta_0 - \beta_{-\infty}) + \displaystyle\int_{-\infty}^0 \gamma\left(-\frac{x_1}{d}\right) d\xi_y - \int_{-\infty}^0 \gamma\left(-\frac{x_1 - 1}{d}\right) d\xi_y \right] \right\} \end{cases} \tag{14}$$

And using numerical methods described in the next section (5) this system can be solved, once these functions ρ_{ti} and ρ_{bi} are known I can solve for f at any point and from that the hydrodynamic fields can be calculated as shown in the next subsection 4.2.

4.2 Hydrodynamic Fields Expression

Using the solved distribution functions, macroscopic quantities such as velocity and density are computed. These fields are critical for evaluating aerodynamic forces and characterizing flow behavior between and around the airfoils.

$$\rho = \int f d\boldsymbol{\xi} \tag{15}$$

$$u_x \cdot \rho = \int \xi_x f d\boldsymbol{\xi} \tag{16}$$

$$u_y \cdot \rho = \int \xi_y f d\boldsymbol{\xi} \tag{17}$$

$$P_{yy}/m = \int (\xi_y - u_y)^2 f d\boldsymbol{\xi} \tag{18}$$

$$P_{xy}/m = \int (\xi_x - u_x)(\xi_y - u_y) f d\boldsymbol{\xi} \tag{19}$$

In order to calculate the forces acting on the airfoils there is no need to evaluate the entire stress tensor. And more over there is no need to calculate these fields in any point that is not at $y = 0, d$ and $0 < x < 1$. Any way, the expressions for the probability

distribution can be plugged in to equation 15 receive for case 4:

$$\begin{aligned}\rho_4(x,y) = &-\frac{1}{2\sqrt{\pi}}\Bigg\{\int_0^{\infty}\left[\operatorname{erf}\left(u_{y\infty}-\frac{y}{x}\xi_x\right)-\operatorname{erf}\left(u_{y\infty}-\frac{y-d}{x}\xi_x\right)\right]e^{-(u_{x\infty}-\xi_x)^2}\,d\xi_x\\ &+\int_{-\infty}^{0}\left[\operatorname{erf}\left(u_{y\infty}-\frac{y}{x-1}\xi_x\right)-\operatorname{erf}\left(u_{y\infty}-\frac{y-d}{x-1}\xi_x\right)\right]e^{-(u_{x\infty}-\xi_x)^2}\,d\xi_x\Bigg\}\\ &+\frac{1}{2\pi y}\int_0^1\rho_{bi}(x_2)\left[\left(\frac{x-x_2}{y}\right)^2+1\right]^{-1}dx_2\\ &+\frac{1}{2\pi(y-d)}\int_0^1\rho_{ti}(x_3)\left[\left(\frac{x_3-x}{y-d}\right)^2+1\right]^{-1}dx_3\end{aligned} \tag{20}$$

In order to get the proper value of the density at a point I first need to solve for ρ_{ti} and ρ_{bi} using section 4.1. Only then its possible to use a numerical method in order to integrate and receive an approximated value. Now this value can be used to calculate the venosity using equations 16,17 and so on for any case described in appendix A. For the values at $y = 0, d$ I cannot use the calculation from equation 20 and I need to address separately although in a very similar fashion. Once the values for the relevant stress components have been calculated it is possible to integrate along every point on the airfoils and get the forces acting on the configuration.

5 Numerical Calculations

5.1 Discretization and Implementation

In order to solve any of the above numerically first the space was discretisize into individual point rather then a continuum. The point are in a constant intervals of x and y where these intervals are h_x and h_y. all integrals that are not solved analytically will be solved using the trapezoid method of integration so I'd expect to have more accurate solutions for these when the intervals h_x and h_y are as small as possible.

5.2 Jacobi Method and Effects

The method used to solve the system 14 is Jacobi's method where I start with an initial guess for $\rho_{ti}^{(0)}(x)$ and use that to solve for $\rho_{bi}^{(0)}$. Then I can iteratively plug our latest version of functions $\rho_{ti}^{(n)}(x), \rho_{bi}^{(n)}$ to find the next set notioned with $n+1$. This iterative process shall take place until a certain condition is met, this may be a number of different thing but I've settled on:

$$\sqrt{\left[\rho_{ti}^{(n+1)}(x)-\rho_{ti}^{(n)}(x)\right]^2+\left[\rho_{bi}^{(n+1)}(x)-\rho_{bi}^{(n)}(x)\right]^2}<\varepsilon \text{ for every } x \tag{21}$$

After some analysis where results with different values for h_x and ε were compered with each other and a conversion to a single solution was detected (for any set of physical

parameters $\tau_t, \tau_b, \boldsymbol{u_\infty}, d$) I concluded that for $h_x < 0.01$ and $\varepsilon < 10^{-6}$ gives a good balance between accurate results and a manageable run time.

5.3 Hydrodynamic Fields Calculation

To solve for the Hydrodynamic fields I used as mentioned the transposed method of integration and for any point (x_1, y_1) I calculated the properties ρ and $\boldsymbol{u}$ and for the point where $y_1 = 0, d$ the stress components P_{yy} and P_{xy} were calculated as well. With those the forces could be evaluated in the same method of integration. A numerical outcome of our method was that at points close to the airfoils (at y values close to 0 or d) I get a very large values in absolute value for ρ in a way that seems to be an error caused by the $1/2\pi y$ factor or $1/2\pi(y-d)$ that become very big while the integral that multiply it depended on h_x and isn't sensitive to h_y in the same manner. In order to fix that problem I made sure to keep that relation

$$\frac{h_x}{h_y} < 0.1 \tag{22}$$

6 Results and Discussion

In order to self check My results at different stages of the project I compered it with well known result and trivial cases. For example, indeed, when I set $\tau_t = \tau_b = 1$ and $\boldsymbol{u_\infty} = 0$ the results are the trivial solution where $\rho = 1$ and $\boldsymbol{u} = \boldsymbol{F} = 0$. In the same comparative fashion, I tested the y component of the macroscopic velocity at $y = 0, d$ to verify that the impermeability condition is satisfied. Next I compered My solution of the force and flow field when d was set to a very large number such as 10 or 100 and indeed My solution converged with the solution for one flat airfoil in the free stream of rarefied gas flow. The next few figures show some results of the flow field and My results for the forces acting on the airfoil configuration. Figure 4 illustrates the flow field for a specific set of conditions: the free-stream velocity is half of the most probable microscopic particle velocity. These results are presented at various angles of attack, with the top airfoil maintained at the free-stream temperature and the bottom airfoil heated to five times that temperature. The vertical distance between the two airfoils is set to 0.45 times the chord length. The figure clearly highlights the stagnation points and regions of flow separation. Notably, while flow separation occurs between the airfoils, it is absent above them.

In addition to analyzing the flow field, the forces acting on the airfoils were calculated under these conditions. The results of these force calculations are summarized in Table 1, providing a detailed breakdown of the forces in both the x and y directions for each airfoil.

Angle (°)	F_{top}		F_{bottom}		F_{total}	
	Drag	Lift	Drag	Lift	Drag	Lift
30	0.4361	0.5877	0.3563	0.4324	0.7924	1.0201
60	0.6176	0.4143	0.848	0.5602	1.4656	0.9745
80	0.6577	0.1585	1.0928	0.2387	1.7505	0.3972

Table 1: Forces on two airfoils at different angles.

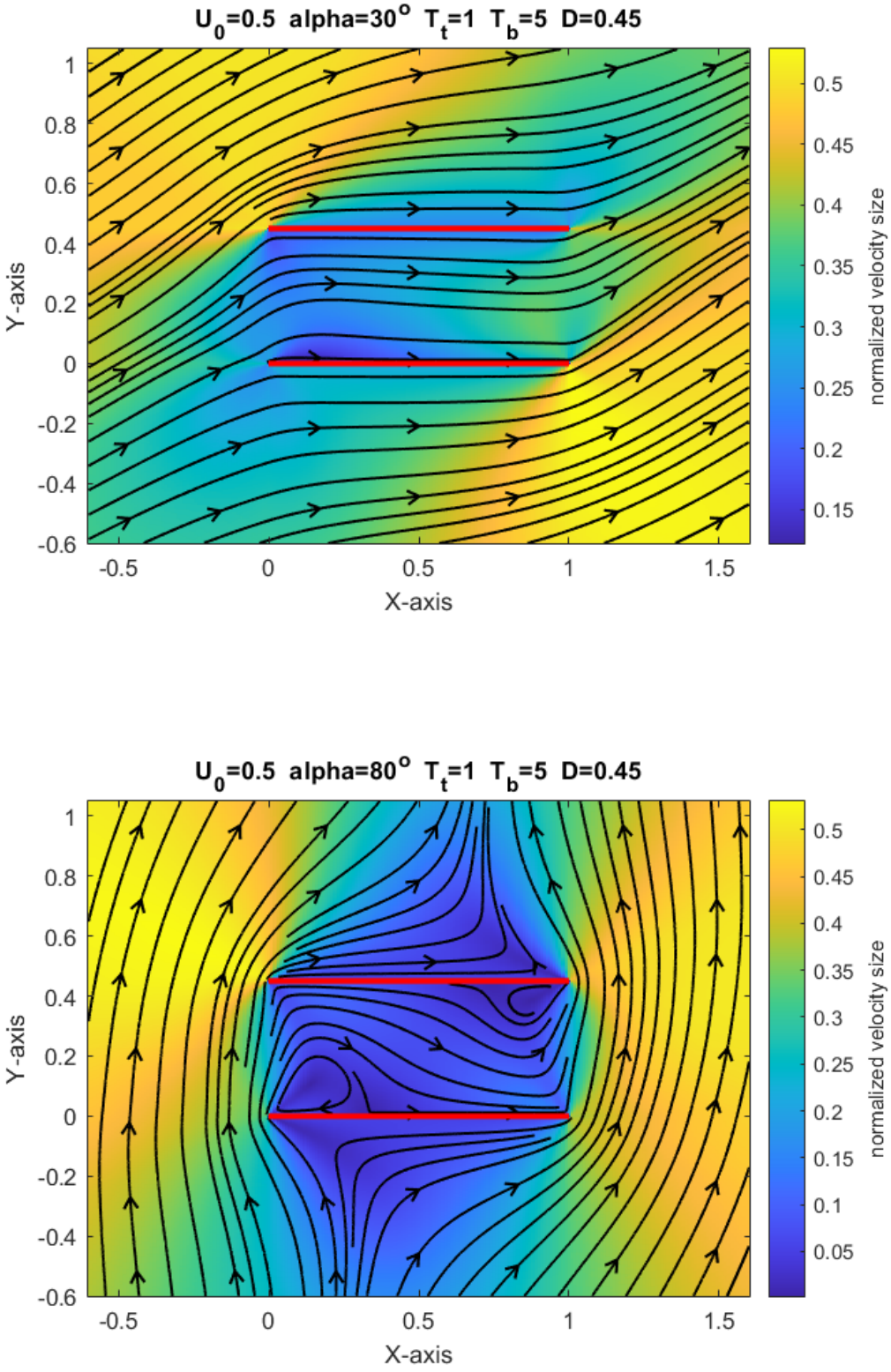

Figure 4: Flow field at different angles of attack

Figures 7 and 5 present similar results for a fixed angle of attack of 60 degrees, including a visualization of the density field and the corresponding stress distributions on the airfoils. These figures provide further insight into the interaction of the flow with the airfoil surfaces under this specific angle of attack.

Finally, Figures 6 and 8 explore how the forces acting on the configuration depend on various parameters. These results highlight the sensitivity of the aerodynamic forces to changes in the governing variables, offering valuable information for understanding the underlying flow physics.

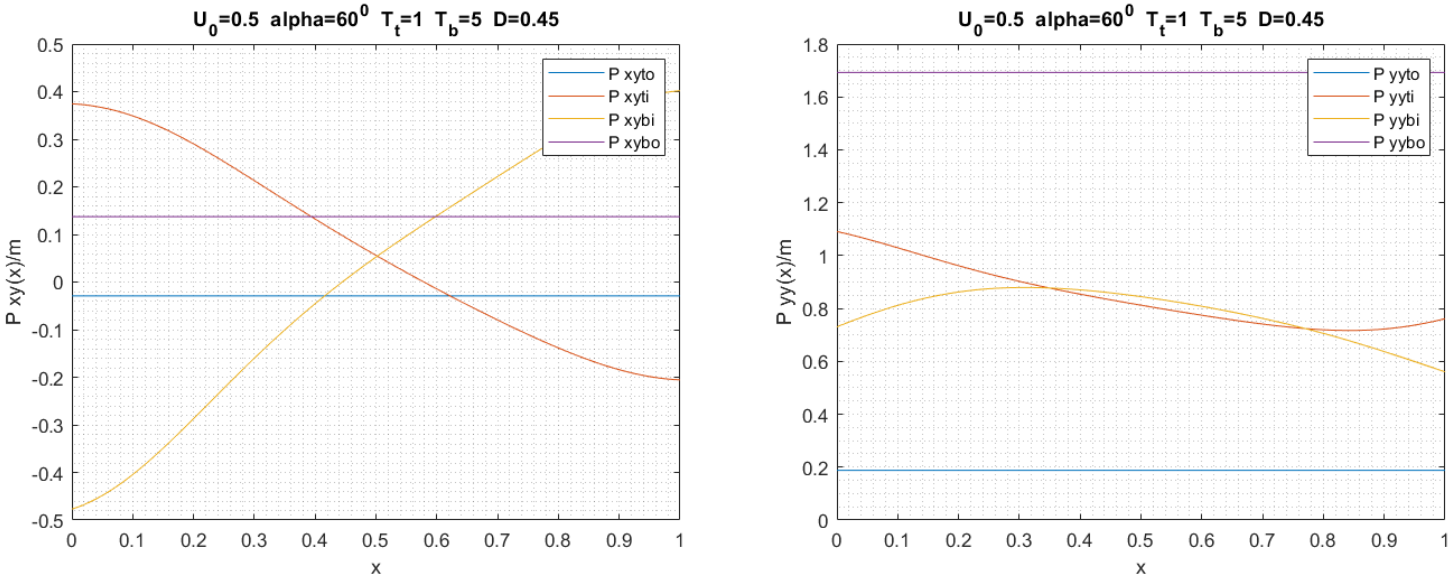

P_{xy} P_{yy}

Figure 5: Stress elements on the airfoils

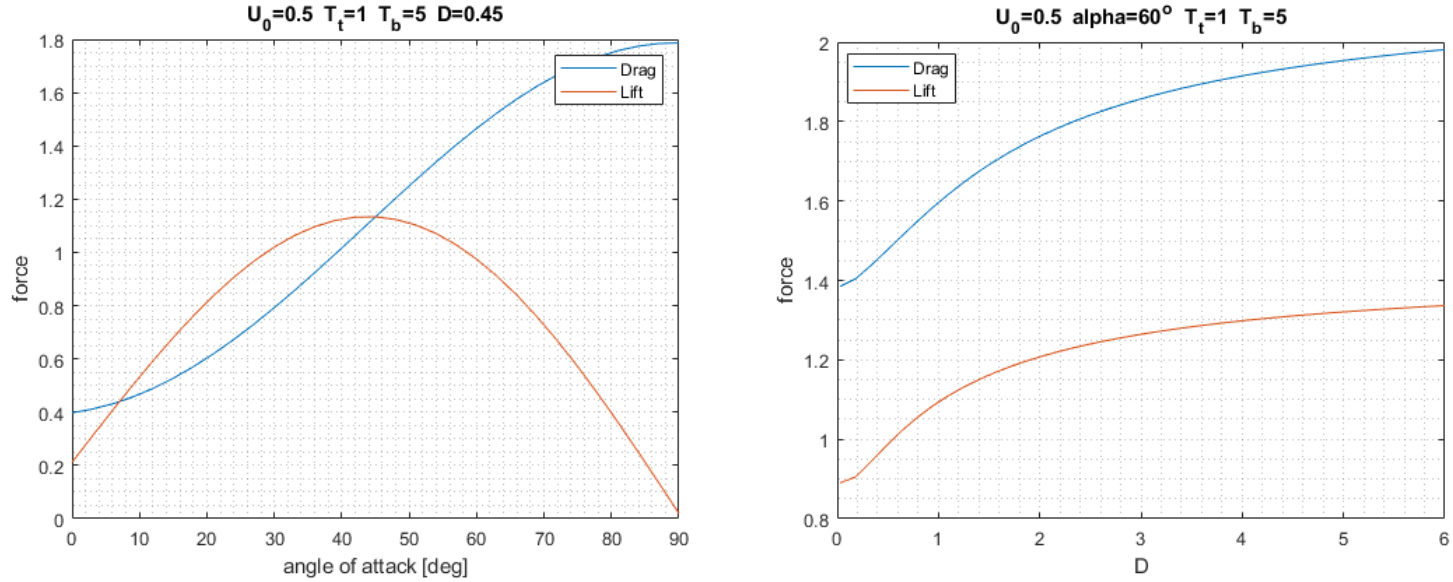

angle of atack distance between the airfoils

Figure 6: Force dependency on geometry variables

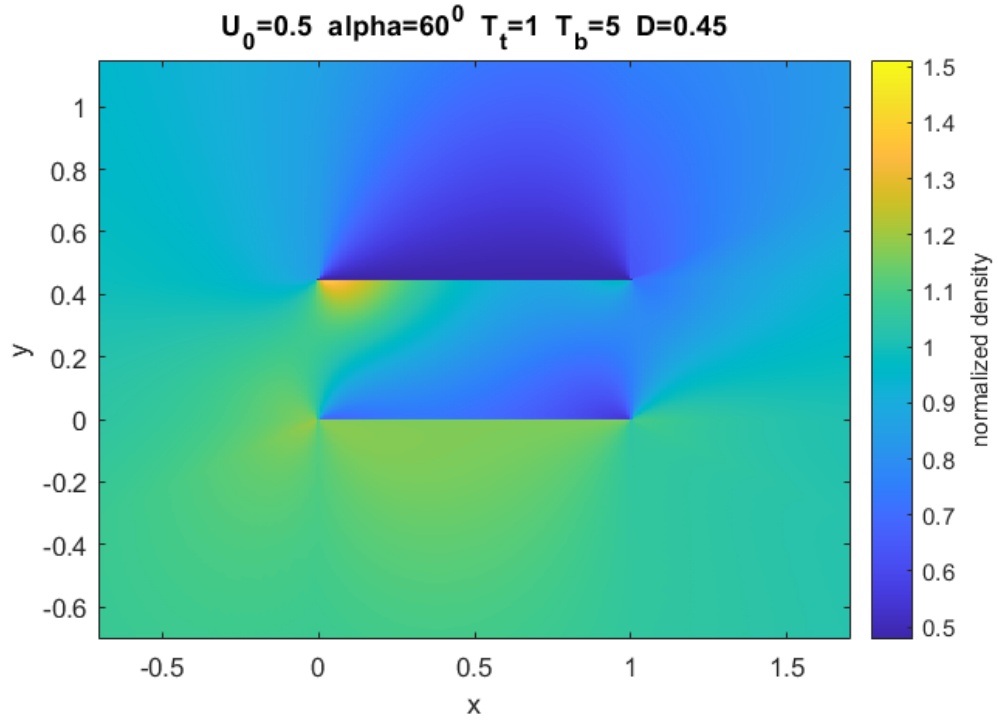

density field

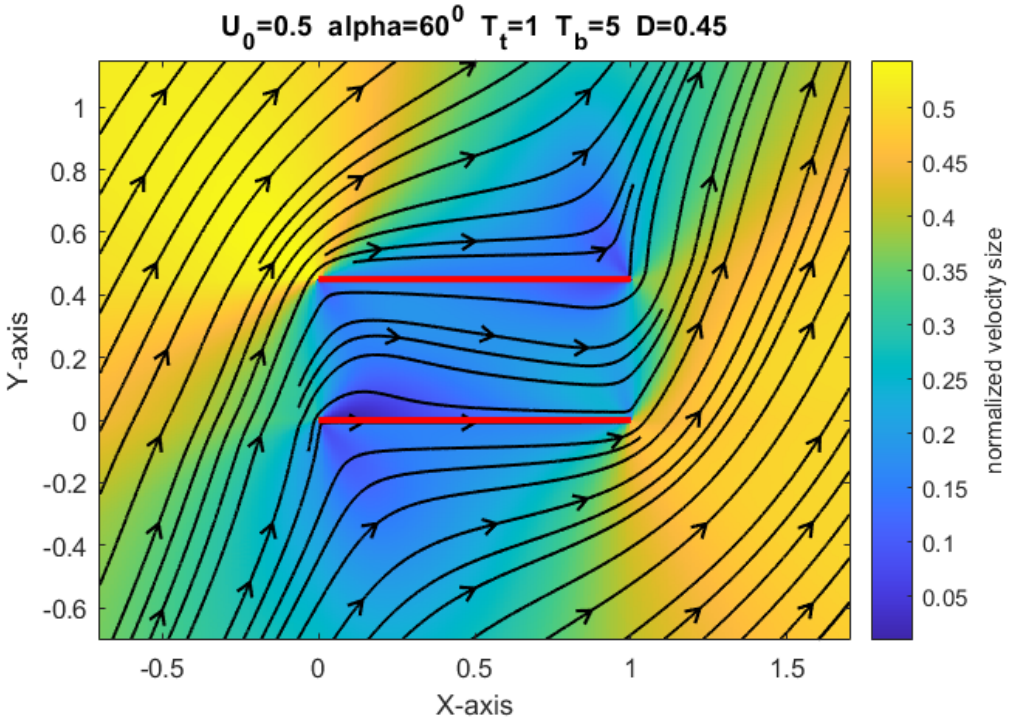

Flow field

Figure 7: hydrodynamic fields at $aoa = 60^o$

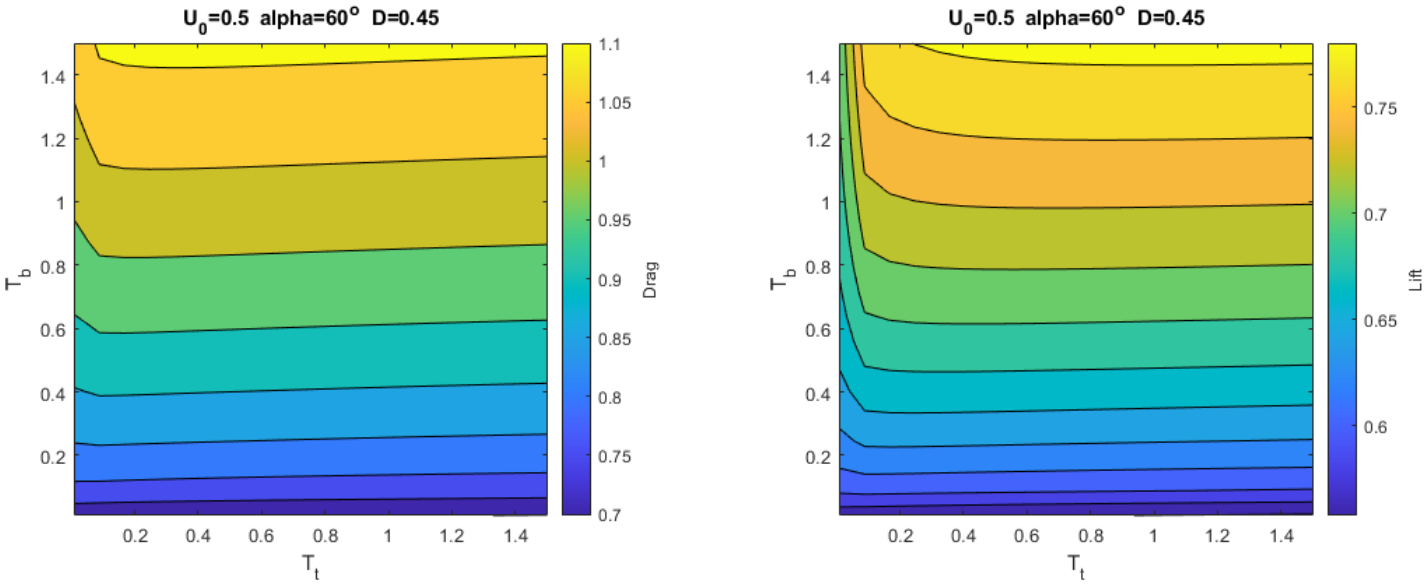

Drag Lift

Figure 8: Force dependency on airfoils temperatures

Some key features that are observed include:

- The lift coefficient at zero angle of attack is not zero although the configuration is geometrically symmetrical. this is due to the high temperature of the bottom airfoil relative to the top one.
- The lift coefficient peaks at angle of attack around 45 degrees before flow separation occurs.
- The maximum value for lift to drag ratio is given at angle of attack of $\approx 23^o$ and is approximately ≈ 1.45.
- As expected, the force has a finite limit as D goes to infinity. This limit has been calculated and compered with the sum of the two airfoils solutions independently (as described in the beginning of section 6), because as D grows the effect of the airfoils on each other is diminishing.
- Most of the effect of the temperatures on the forces is from the bottom airfoils temperature.
- Surprisingly the effect of the top airfoils temperature does not effect the forces acting upon the configuration beyond a value around 1.5 times the ambient temperature unlike the effect of the bottom airfoils temperature.

7 Future Work

Future work could involve a more in-depth exploration of the current results while extending the analysis to include specular wall boundary conditions. This modification would provide insights into how different wall interaction models influence the flow dynamics and force distributions. Additionally, a fascinating direction for further study would be

to compare these findings with the results obtained in the limit as $Kn \to 0$, which corresponds to the continuum regime. Such a comparison could reveal the extent to which rarefaction effects play a role in shaping the flow behavior and aerodynamic forces.

Moreover, investigating the transitional regime between rarefied and continuum conditions could provide a broader understanding of the problem. This might include studying how the force coefficients, flow separation patterns, and stagnation point locations evolve as the Knudsen number decreases. Incorporating different angles of attack, wall temperatures, or configurations could add valuable perspectives.

Additionally, it would be worthwhile to examine the computational challenges associated with modeling this problem in the continuum limit, such as the increased demands for grid resolution or the need for advanced numerical methods. Comparing the accuracy and computational efficiency of various modeling approaches (e.g., direct simulation Monte Carlo vs. Navier-Stokes solvers) could further contribute to the body of knowledge in this field.

References

[1] Sun X-Y, Li T-E, Lin G-C, Wu Y. *A study on the aerodynamic characteristics of a stratospheric airship in its entire flight envelope.* ,2017.

[2] Bullard, Jacob. *Satellite Drag Analysis using Direct Simulation Monte Carlo (DSMC).* ,2018.

[3] G. A. Bird, *Molecular Gas Dynamics and the Direct Simulation of Gas Flows*, 1994.

[4] F. Sharipov, *Rarefied Gas Flow Through Channels* 2012.

Appendix A

case 1

In this case the point is above the top airfoil and only sees the top one.

$$f_1(x_1, y_1, \boldsymbol{\xi}) = \begin{cases} f_{to} & \text{if } \xi_y > 0 \quad \text{and} \quad \frac{x_1-1}{y_1-d}\xi_y < \xi_x < \frac{x_1}{y_1-d}\xi_y \\ f_\infty & \text{otherwise} \end{cases}$$

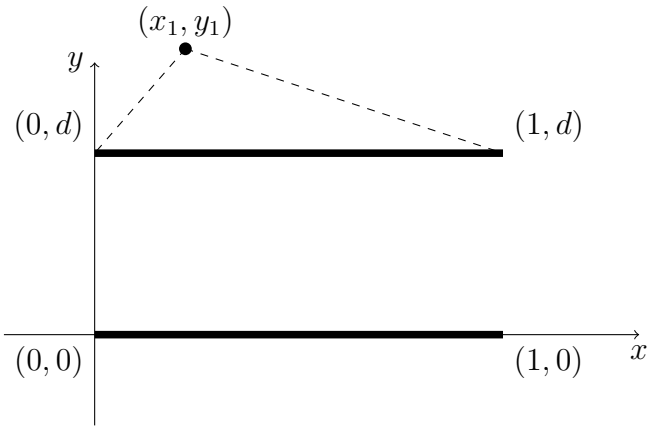

case 2 and 2'

In this case the point is above the top airfoil and sees a part of the bottom one.

$$f_2(x_1, y_1, \boldsymbol{\xi}) = \begin{cases} f_{to} & \text{if } \xi_y > 0 \quad \text{and} \quad \frac{x_1-1}{y_1-d}\xi_y < \xi_x < \frac{x_1}{y_1-d}\xi_y \\ f_{bi} & \text{if } \xi_y > 0 \quad \text{and} \quad \frac{x_1-1}{y_1}\xi_y < \xi_x < \frac{x_1-1}{y_1-d}\xi_y \\ f_\infty & \text{otherwise} \end{cases}$$

$$f_2'(x_1', y_1', \boldsymbol{\xi}) = \begin{cases} f_{to} & \text{if } \xi_y > 0 \quad \text{and} \quad \frac{x_1'-1}{y_1'-d}\xi_y < \xi_x < \frac{x_1'}{y_1'-d}\xi_y \\ f_{bi} & \text{if } \xi_y > 0 \quad \text{and} \quad \frac{x_1'}{y_1'-1}\xi_y < \xi_x < \frac{x_1'}{y_1'-d}\xi_y \\ f_\infty & \text{otherwise} \end{cases}$$

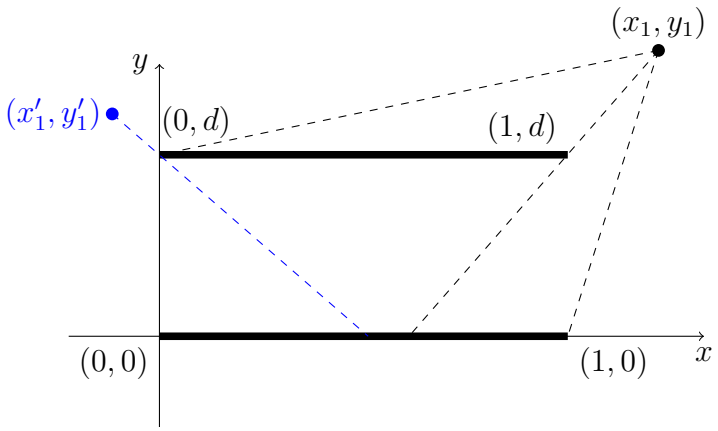

case 3

In this case the point is above the top airfoil and sees all of the bottom one.

$$f_3(x_1, y_1, \boldsymbol{\xi}) = \begin{cases} f_{to} & \text{if } \xi_y > 0 \quad \text{and} \quad \frac{x_1-1}{y_1-d}\xi_y < \xi_x < \frac{x_1}{y_1-d}\xi_y \\ f_{bi} & \text{if } \xi_y > 0 \quad \text{and} \quad \frac{x_1-1}{y_1}\xi_y < \xi_x < \frac{x_1}{y_1}\xi_y \\ f_\infty & \text{otherwise} \end{cases}$$

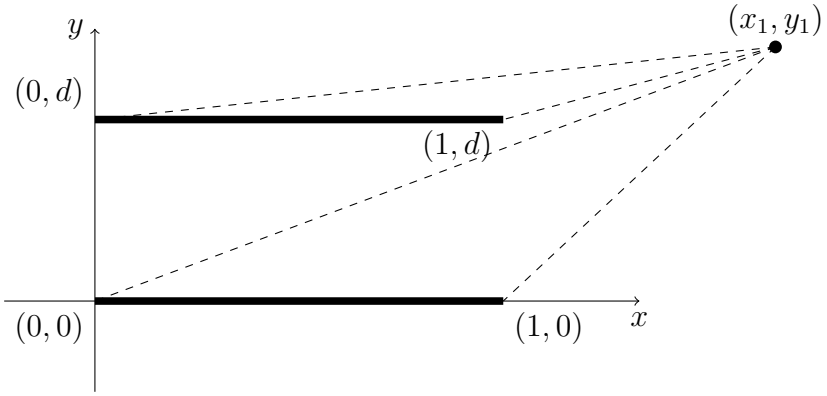

case 4

In this case the point is between the airfoils.

$$f_4(x_1, y_1, \boldsymbol{\xi}) = \begin{cases} f_\infty & \text{if } \xi_x > 0 \quad \text{and} \quad \frac{y_1-d}{x_1}\xi_x < \xi_y < \frac{y_1}{x_1}\xi_x \\ & \text{or} \\ & \text{if } \xi_x < 0 \quad \text{and} \quad \frac{y_1-d}{x_1-1}\xi_x < \xi_y < \frac{y_1}{x_1-1}\xi_x \\ f_{ti} & \text{if } \xi_y < 0 \quad \text{and} \quad \frac{x_1}{y_1-d}\xi_y < \xi_x < \frac{x_1-1}{y_1-d}\xi_y \\ f_{bi} & \text{if } \xi_y > 0 \quad \text{and} \quad \frac{x_1-1}{y_1}\xi_y < \xi_x < \frac{x_1}{y_1}\xi_y \end{cases}$$

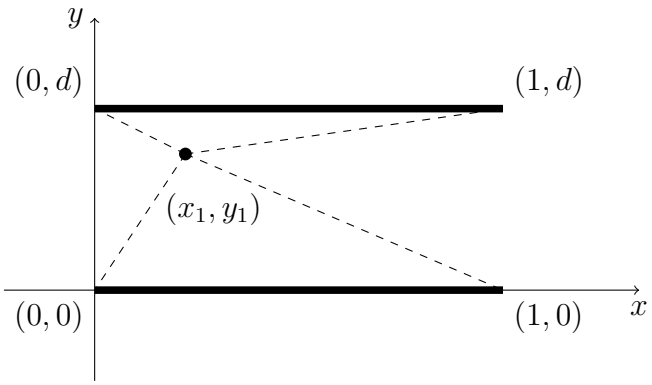

case 5

In this case the point is above the top airfoil and only sees the top one.

$$f_5(x_1, y_1, \boldsymbol{\xi}) = \begin{cases} f_{ti} & \text{if } \xi_y < 0 \quad \text{and} \quad \frac{x_1-1}{y_1-d}\xi_y < \xi_x < \frac{x_1}{y_1-d}\xi_y \\ f_{bo} & \text{if } \xi_y < 0 \quad \text{and} \quad \frac{x_1-1}{y_1}\xi_y < \xi_x < \frac{x_1}{y_1}\xi_y \\ f_\infty & \text{otherwise} \end{cases}$$

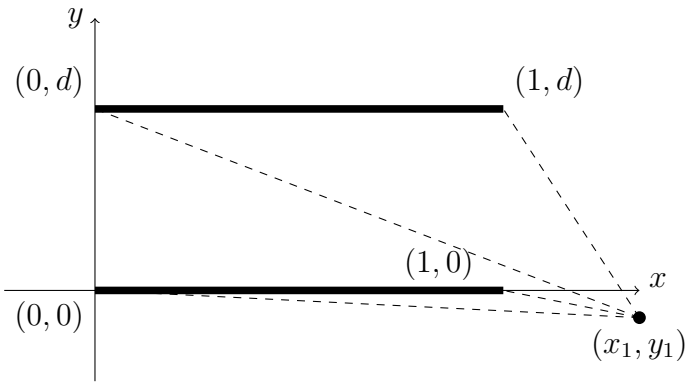

case 6 and 6'

In this case the point is above the top airfoil and only sees the top one.

$$f_6(x_1, y_1, \boldsymbol{\xi}) = \begin{cases} f_{ti} & \text{if } \xi_y < 0 \quad \text{and} \quad \frac{x_1-1}{y_1-d}\xi_y < \xi_x < \frac{x_1-1}{y_1}\xi_y \\ f_{bo} & \text{if } \xi_y < 0 \quad \text{and} \quad \frac{x_1-1}{y_1}\xi_y < \xi_x < \frac{x_1-1}{y_1}\xi_y \\ f_\infty & \text{otherwise} \end{cases}$$

$$f'_6(x'_1, y'_1, \boldsymbol{\xi}) = \begin{cases} f_{ti} & \text{if } \xi_y < 0 \quad \text{and} \quad \frac{x'_1}{y'_1}\xi_y < \xi_x < \frac{x'_1}{y'_1-d}\xi_y \\ f_{bo} & \text{if } \xi_y < 0 \quad \text{and} \quad \frac{x'_1-1}{y'_1}\xi_y < \xi_x < \frac{x'_1}{y'_1}\xi_y \\ f_\infty & \text{otherwise} \end{cases}$$

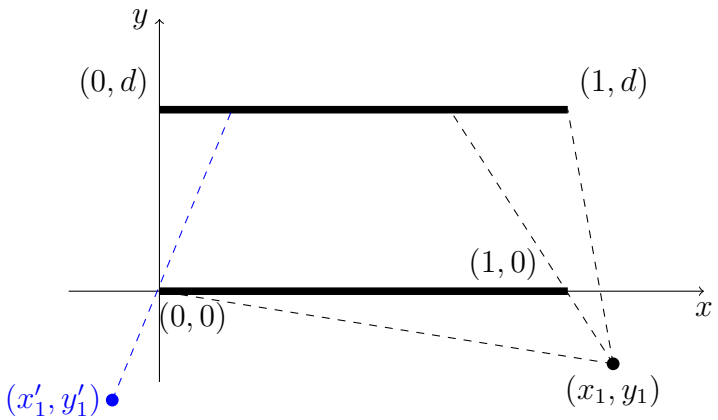

case 7

In this case the point is below the bottom airfoil and only sees the bottom one.

$$f_7(x_1, y_1, \boldsymbol{\xi}) = \begin{cases} f_{bo} & \text{if } \xi_y < 0 \quad \text{and} \quad \frac{x_1-1}{y_1}\xi_y < \xi_x < \frac{x_1}{y_1}\xi_y \\ f_\infty & \text{otherwise} \end{cases}$$

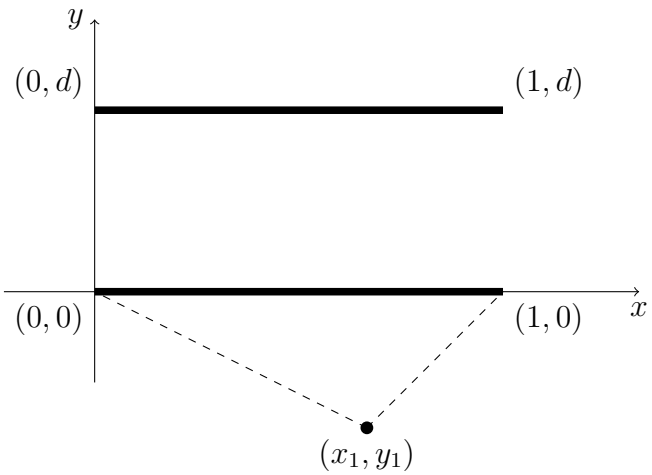
y
$(0, d)$
$(1, d)$
$(0, 0)$
$(1, 0)$
x
(x_1, y_1)